

Simulation and Analysis of Pose Setting Test of Space Redocking Manipulator End-effector Based on Parallel Mechanism

Xinlin Bai

State Key Laboratory of Robotics, Shenyang Institute of Automation, Chinese Academic of Sciences, Shenyang, China
Email: baixinlin@sia.cn

Zhigang Xu^{1,2}, Mingyang Liu¹, Meng Yin^{1,2}

¹State Key Laboratory of Robotics, Shenyang Institute of Automation, Chinese Academic of Sciences, Shenyang, China

²University of Chinese Academy of Sciences, Beijing, China

Email: {zgxu, liumingyang, yingmeng}@sia.cn

Abstract—According to pose setting ground test requirements of space station redocking manipulator end-effector, a method based on parallel mechanism is proposed to meet the demand between actuator and adapter. Firstly, Parallel mechanism of 6-DOF is designed and its working principle of pose setting is described. Secondly, mathematical models of parallel mechanism agile space, kinematic interference characteristics of actuator and adapter and structural statics are established. Finally, workspace search algorithm base on cylindrical coordinates and interference detection algorithm using space geometry are programmed by Matlab, respectively. Simulation results show that movement range of designed parallel mechanism can satisfy the demand of required pose, there is no motion interference between driving branches and adapter, mechanism has good bearing capacity, and the method is also effective.

Index Terms—space station Redocking manipulator, end-effector, pose setting, parallel mechanism

I. INTRODUCTION

China plans to establish and operate the Low Earth Orbit (LEO) space station around 2020 [1], which is a milestone in the development of long-term manned space technology. Space station redocking manipulator is a key space mechanism to assemble modular space station, which transfers an active docking cabin from axis lord docking port to radial berthing port of target module[2]. End-effector, mainly consisting of actuator attached to the end of manipulator arm and adapter fixed to the target module, is the core connecting component of the redocking manipulator. A connection deviation, generally six dimensional spatial position and attitude error, occurs inevitably during the operation of actuator and adapter. In order to ensure successful establishment of space station avoiding significant losses, pose setting ground test is conducted to examine error tolerance performance of

actuator and adapter or modify their design parameters [3, 4].

Russia and the United States pioneer the construction of the space station and its supporting ground experiment research work. End-effector pose setting method of space manipulator has been reported and studied in ground test of United States and Russia [5, 6]. A variety of experimental studies are carried out on auxiliary maintenance manipulator end-effector of Hubble space telescope (HST) before being launched into space and the implementations of space precision parts replacement and maintenance operations [7]. Prototype tests of large space mechanical arms equipped with space shuttle Buran are also performed, which includes tolerance connection experiments of the end effector, but the test method and working principle in detail have not been elaborated [8]. Space station redocking manipulator of China is still in development phase. As mentioned in [9-10], the three dimensional relative pose between actuator and adapter can be set through mounting on different frames during the test of a certain type of space arm end-effector, while the pose accuracy and experiment efficiency is low.

According to the position and attitude test requirements of the manipulator end-effector, a pose setting method based on parallel mechanism is proposed. Parallel mechanism, widely used in many precision fields, has high accuracy and rigidity with smaller space implementation volume, which is more advantageous than serial mechanism and hybrid mechanism in pose setting ground test [11-13]. In the paper, pose setting working principle using 6-DOF parallel mechanism is described, mathematical models of parallel mechanism agile space, kinematic interference characteristics of actuator and adapter and structural statics are also established and the proposed method is verified by simulation.

II. MECHANICAL DESIGN OF PARALLEL MECHANISM

The designed parallel mechanism can be divided into three parts, moving platform, static platform and driving

branches. There are six driving branches between moving platform and static platform. Both ends of each driving branch are equipped with high precision Hooke hinges, which are distributed on the circumference of moving platform and static platform respectively. The structure diagram of parallel mechanism is shown in Fig. 1.

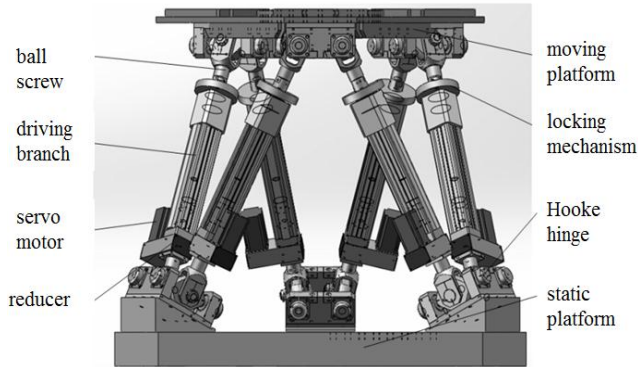


Figure 1. The structure diagram of parallel mechanism

The designed parallel mechanism is a 6-DOF mechanism concluded from screw theory and structure constraints [14-16]. Moving platform can achieve linear motion, rotary motion and the combination of the two movement forms, which meets the free degree and movement function requirements of space redocking manipulator end-effector ground pose setting test.

III. POSE SETTING TEST PRINCIPLE OF SPACE STATION REDOCKING MANIPULATOR END-EFFECTOR

In the process of end-effector pose setting test of space station redocking manipulator, adapter is installed on the moving platform and actuator is located at the end of the manipulator. Six dimensional relative spatial position and attitude error between adapter and actuator, occurred in space redocking, can be precisely set. Fig. 2 shows pose setting principle of end-effector using parallel mechanism.

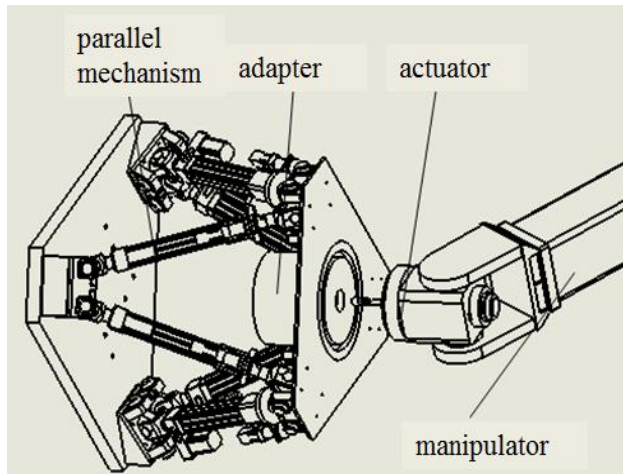


Figure 2. Pose setting principle of end-effector using parallel mechanism

When a specific pose experiment is carried out, the linear displacement of each driving branch is calculated through kinematic mathematical model of parallel

mechanism, and the linear displacements are converted into rotation angles of the servo motors by host computer. The control system changes the length of each single branch by driving corresponding servo motor. Each driving branch is equipped with a linear grating ruler, which provides position closed-loop feedback for drive control system. The spatial position and posture of control point located on adapter constantly changes until the preset value are reached. The actuator will successively implement a series of operations (like capture, connection and lock, etc.) to the adapter after the completion of above pose setting process.

IV. MATHEMATICAL MODELING OF KINEMATICS AND STATICS OF PARALLEL MECHANISM

A. Kinematic Modeling of Agile Space

In order to analyze the agile space and deduce the kinematic model, mechanism schematic is essential and can be obtained by simplifying the structure of parallel mechanism. The coordinate systems are established, as seen in Fig. 3. $\{O_{sx} - X_{sx} Y_{sx} Z_{sx}\}$ is the coordinate system of static platform and $\{O_{ss} - X_{ss} Y_{ss} Z_{ss}\}$ is the coordinate system of moving platform. $A_1 \sim A_6$ and $B_1 \sim B_6$ are rotation centers of Hooke angular in moving platform and static platform respectively. R_{ss} is radius of the circle of A_i and R_{sx} is the radius of the circle of B_i . The angles between adjacent Hooke hinges in moving platform and static platform are α_{ss} and α_{sx} . The projection of $\{O_{sx} - X_{sx} Y_{sx} Z_{sx}\}$ and $\{O_{ss} - X_{ss} Y_{ss} Z_{ss}\}$ in the XOY plane are coincident in the initial condition.

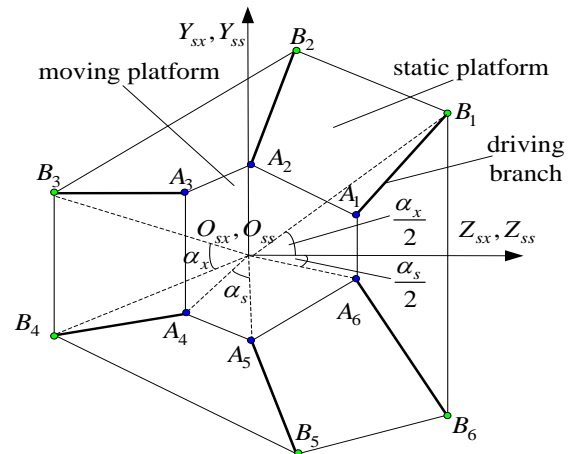


Figure 3. The coordinate systems of parallel mechanism

The coordinates of B_i in $\{O_{sx} - X_{sx} Y_{sx} Z_{sx}\}$ and the coordinates of A_i in $\{O_{ss} - X_{ss} Y_{ss} Z_{ss}\}$ can be obtained as follows:

$$\mathbf{A}_s = [A_1 \ A_2 \ A_3 \ A_4 \ A_5 \ A_6] \quad (1)$$

$$\mathbf{B}_x = [B_1 \ B_2 \ B_3 \ B_4 \ B_5 \ B_6] \quad (2)$$

Here, the expressions of A_i and B_i are

$$A_i = \begin{bmatrix} R_{ss} \cdot \cos\left(\frac{2i-1+(-1)^{i-1}}{6}\pi + (-1)^i \cdot \frac{\alpha_{ss}}{2}\right) \\ R_{ss} \cdot \sin\left(\frac{2i-1+(-1)^{i-1}}{6}\pi + (-1)^i \cdot \frac{\alpha_{ss}}{2}\right) \\ 0 \end{bmatrix} \quad (3)$$

$$B_i = \begin{bmatrix} R_{sx} \cdot \cos\left(\frac{2i-1+(-1)^i}{6}\pi + (-1)^{i-1} \cdot \frac{\alpha_{sx}}{2}\right) \\ R_{sx} \cdot \sin\left(\frac{2i-1+(-1)^i}{6}\pi + (-1)^{i-1} \cdot \frac{\alpha_{sx}}{2}\right) \\ 0 \end{bmatrix} \quad (4)$$

We set the control point P at the center of connecting flange and the position vector of control point P in $\{O_{ss}-X_{ss}Y_{ss}Z_{ss}\}$ is

$$\mathbf{P}_s = \mathbf{T}_s \cdot [x_p, y_p, z_p]^T + [0, 0, H_s]^T \\ = [P_{sx}, P_{sy}, P_{sz}]^T \quad (5)$$

Here, the coordinate of P in coordinate system $\{O_{ss}-X_{ss}Y_{ss}Z_{ss}\}$ is $[x_p, y_p, z_p]^T$, the initial distance between static platform and moving platform is H_s , the attitude angles of roll, pitch and yaw of moving platform are α_s , β_s and γ_s respectively, the translation matrix is $\mathbf{T}_s = \mathbf{T}_1\mathbf{T}_2\mathbf{T}_3$, \mathbf{T}_1 , \mathbf{T}_2 and \mathbf{T}_3 can be described as

$$\mathbf{A}_1 = \begin{bmatrix} 1 & 0 & 0 \\ 0 & \cos \alpha_s & -\sin \alpha_s \\ 0 & \sin \alpha_s & \cos \alpha_s \end{bmatrix} \quad (6)$$

$$\mathbf{A}_2 = \begin{bmatrix} \cos \beta_s & 0 & \sin \beta_s \\ 0 & 1 & 0 \\ -\sin \beta_s & 0 & \cos \beta_s \end{bmatrix}$$

$$\mathbf{A}_3 = \begin{bmatrix} \cos \gamma_s & -\sin \gamma_s & 0 \\ \sin \gamma_s & \cos \gamma_s & 0 \\ 0 & 0 & 1 \end{bmatrix}$$

Similarly, we get the position vector \mathbf{A}_{xs} of point A_i to point A_6 .

$$\mathbf{A}_{xs} = \mathbf{T}_s \cdot \mathbf{A}_s + [0, 0, H_s]^T \quad (7)$$

Assume l_{si} is the length of each driving branch and it changes when moving platform is tested in different pose. In any state, l_{si} can be given by $|\mathbf{A}_{xs}(i)\mathbf{B}_x(i)|$ and \mathbf{I}_s , length matrix of driving branches, can be written as

$$\mathbf{I}_s = [|\mathbf{A}_{xs}(1)\mathbf{B}_x(1)|, |\mathbf{A}_{xs}(2)\mathbf{B}_x(2)|, |\mathbf{A}_{xs}(3)\mathbf{B}_x(3)|, \\ |\mathbf{A}_{xs}(4)\mathbf{B}_x(4)|, |\mathbf{A}_{xs}(5)\mathbf{B}_x(5)|, |\mathbf{A}_{xs}(6)\mathbf{B}_x(6)|] \quad (8)$$

The maximum value and minimum value of the single branch length are $l_{s\max}$ and $l_{s\min}$, and the following equation holds:

$$l_{s\min} \leq |\mathbf{I}_s|(i) \leq l_{s\max}, i=1, 2, \dots, 6 \quad (9)$$

B. Motion Interference Characteristics Model Between Adapter and Driving Branches

In order to avoid the interference between the bottom of adapter and driving branches and ensure that the end-effector is properly locked and connected during the pose setting test, mechanism analysis and mathematic modeling of motion interference characteristics are essential. Because the envelope shape of the adapter embedded in the internal part of parallel mechanism is a cylinder, we define the maximum envelope outer radius of adapter bottom surface Π_{xj} is R_{xj} . The position vector of adapter bottom center point O_{xj} is \mathbf{O}_{xj} , the maximum envelope radius of single driving branches is R_{sz} . The schematic diagram of motion interference between adapter and driving branches is shown in Fig. 4.

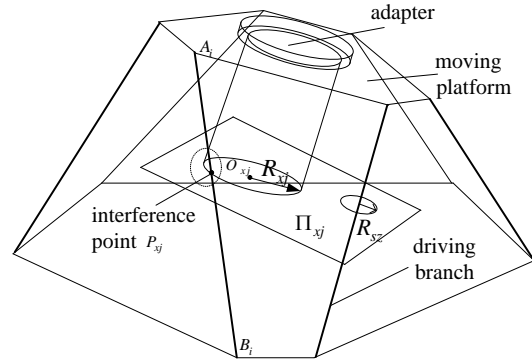


Figure 4. The schematic diagram of motion interference between adapter and driving branches

The intersection point P_{xj} of space line A_iB_i and Π_{xj} is located in the interior of adapter bottom envelope circle during mechanism interference. Thus, the geometric constraint without motion interference is

$$|O_{xj}P_{xj}| - R_{xj} - R_{sz} > 0 \quad (10)$$

Intersection point P_{xj} coordinate $\mathbf{P}_{xj} = (x_{xj}, y_{xj}, z_{xj})^T$ can be given by solving the equation of space line A_iB_i and the equation of space plane Π_{xj} .

$$\Pi_{xj} : [A_{xj}, B_{xj}, C_{xj}] \cdot (\mathbf{P}_{xj} - \mathbf{O}_{xj})^T = 0 \quad (11)$$

$$A_iB_i : \frac{x_{xj} - B_{ix}}{A_{ix} - B_{ix}} = \frac{y_{xj} - B_{iy}}{A_{iy} - B_{iy}} = \frac{z_{xj} - B_{iz}}{A_{iz} - B_{iz}} = t \quad (12)$$

Here, A_{ix} , A_{iy} and A_{iz} are the coordinate component of A_{xs} and B_{ix} , B_{iy} and B_{iz} are the coordinate component of B_i .

C. Mathematical Modeling of Mechanism Statics

The parallel platform is subjected to large impact loads during the process of capture, docking and connection in manipulator end-effector pose setting ground test and the loads are directly applying to driving branches and then acting on servo motors. In order to ensure the structure stiffness of parallel mechanism, the output forces of driving branch screws and the stability of pose setting to meet the test requirements, mechanism statics analysis are necessary. F_x, F_y, F_z, M_x, M_y and M_z are six-component force/torque, defined in $\{O_{sx}-X_{sx}Y_{sx}Z_{sx}\}$, applied at control point P . F_i and $\overline{A_iB_i}$ are the pressure and direction vector of driving branch A_iB_i , respectively. If the calculated value of F_i is negative, it indicates that the driving branch is bearing tensile force. We get the equilibrium equations of force and torque as followings:

$$\sum_{i=1}^6 F_i \frac{B_i - A_i}{|A_i B_i|} + \mathbf{F} = 0 \tag{13}$$

$$\sum_{i=1}^6 (O_{sx} A_i - O_{sx} p) \times \left(F_i \frac{B_i - A_i}{|A_i B_i|} \right) + \mathbf{M} = 0 \tag{14}$$

Here, $\mathbf{F} = [F_x, F_y, F_z]^T$ and $\mathbf{M} = [M_x, M_y, M_z]^T$.

V. SIMULATION

In order to prove six dimensional pose setting performance of 6-DOF parallel mechanism, simulations is carried out under the given pose range. The pose setting range of end-effector is shown in Table I.

TABLE I. THE POSE SETTING RANGE OF END-EFFECTOR

Parameter	ΔP_{s_x}	ΔP_{s_y}	ΔP_{s_z}	α_s	β_s	γ_s
Unit	mm	mm	mm	°	°	°
Value	150	±200	±200	±3	±3	±3

A. Agile Space of 6-DOF Parallel Mechanism

The search algorithm based on column coordinate is used to get the agile space of 6-DOF parallel mechanism and its flow chart is shown in Fig. 5.

We can see that the smaller the iteration step, the higher the accuracy of the agile space, while the search time will increase exponentially. So the search step size, $\Delta\alpha_s, \Delta\beta_s, \Delta\gamma_s, r_step$ and $\Delta\theta$ should be chosen reasonably.

Search algorithm is programmed using Matlab according to above pseudo code. Fig. 6, Fig. 7, Fig. 8 and Fig. 9 show the agile space of control point P .

It can be seen from figure 6 to figure 9, coordinate ranges of control point P are $814.519mm \leq P_{s_x} \leq 972.5190mm$, $-252mm \leq P_{s_y} \leq 238mm$ and $-225.5625mm \leq P_{s_z} \leq 225.5625mm$. That means agile space of parallel mechanism, that are $\Delta P_{s_x}, \Delta P_{s_y}$ and ΔP_{s_z} , meet the requirement of pose setting range of space redocking manipulator end-effector.

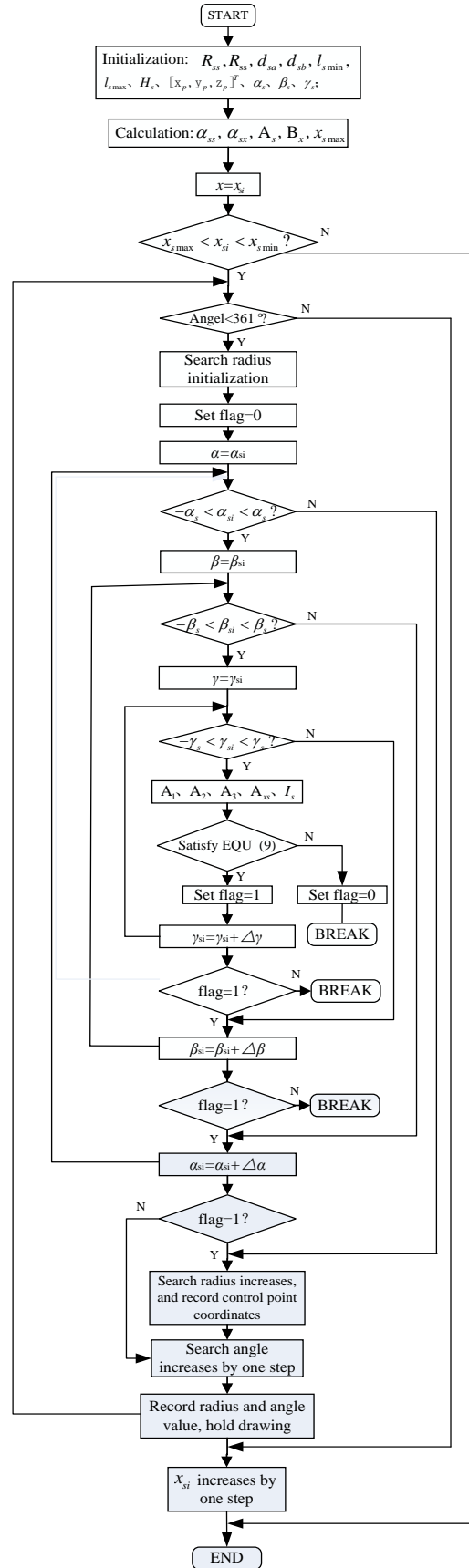


Figure 5. The flow chart of search algorithm

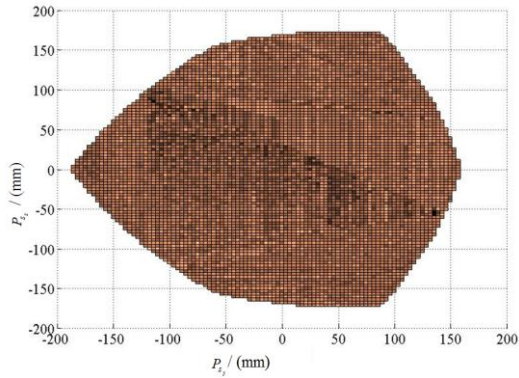


Figure 6. Agile space section when $P_{sx}=900$

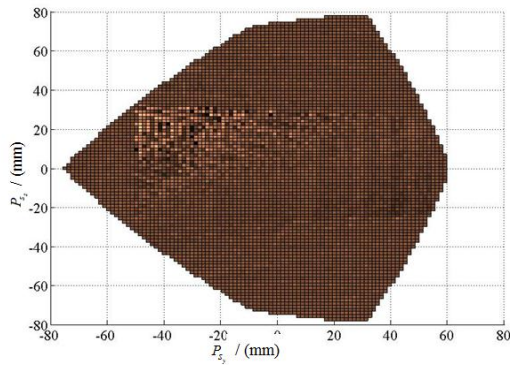


Figure 7. Agile space section when $P_{sx}=950$

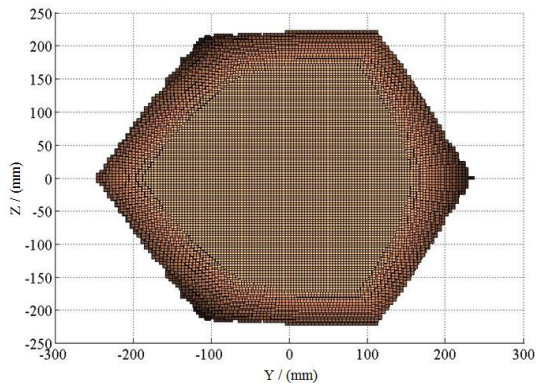


Figure 8. Top view of agile space

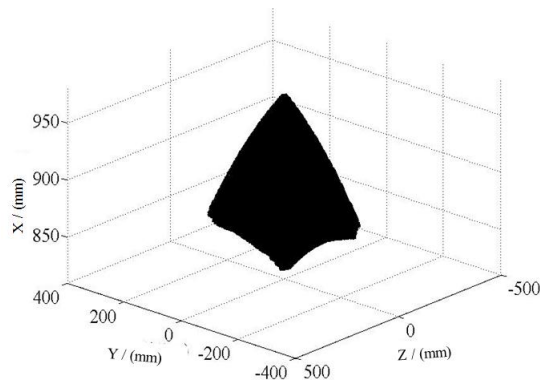


Figure 9. Axonometric drawing of agile space

B. Mechanism Interference Simulation

Interference detection algorithm code in MATLAB can be obtained on the basis of above work by adding the corresponding programs of equation (10) to equation (12). Safe distance d_s between driving branches and adapter is also given in mechanism agile space.

Figure 10 depicts movement trajectory of point O_{sj} and driving branch A_jB_j . We can get the minimum of $|O_{sj}P_{sj}|$ is 269.6802mm and d_s is 64.6802mm. Therefore, six driving branches do not interfere with adapter in pose setting test, which verifies the rationality of structure parameters of the designed parallel mechanism. The main structure parameters of designed parallel mechanism are seen in Table. 2.

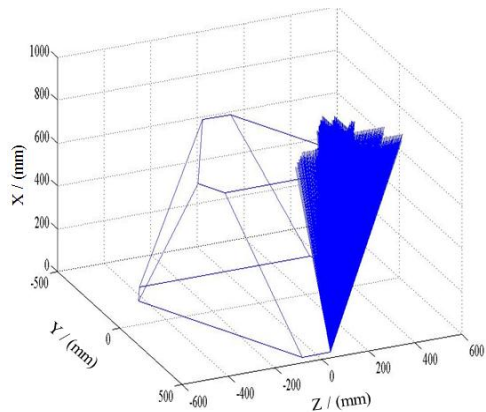
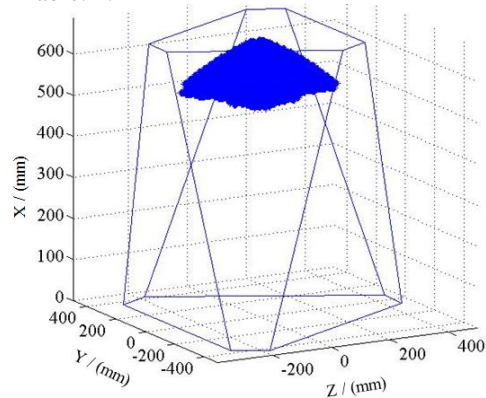


Figure 10. Movement trajectory of point O_{sj} driving branch A_jB_j

TABLE 2. Main structure parameters of designed parallel mechanism

Parameter	R_{sx}	R_{sx}	$l_{s \min}$	$l_{s \max}$	d_{si}	H_s
Unit	mm	mm	mm	mm	mm	mm
Value	350	460	754	964	210	94

C. Simulation of Mechanism Statics Characteristics

When moving platform bears force F and moment M applied at control point p respectively and $P_{sx}=900$, force pole diagrams of driving branches are shown in Fig. 11 and Fig. 12. In the simulation, $F=[1000N, 1000N, 1000N]^T$ and $M=[1000N \cdot m, 1000N \cdot m, 1000N \cdot m]^T$.

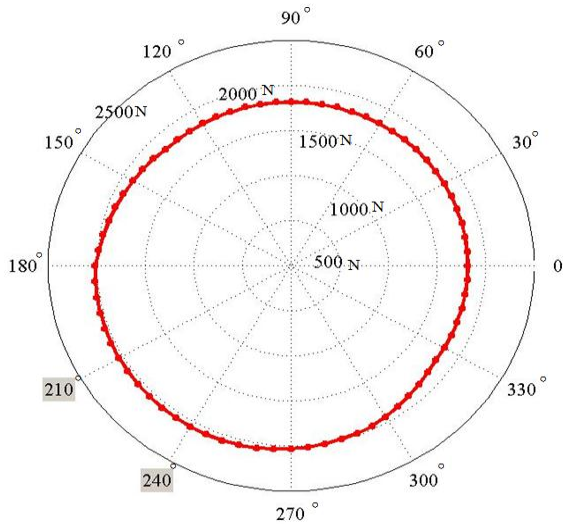


Figure 11. Force pole diagram of driving branches under conditions of F and $P_s = 900$

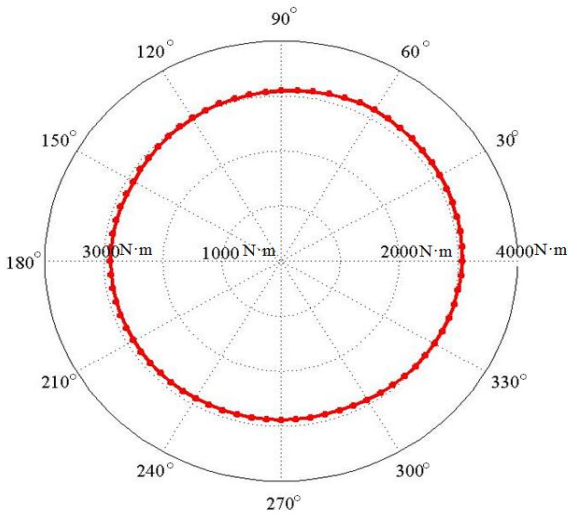


Figure 12. Force pole diagram of driving branches under conditions of M and $P_s = 900$

The maximum force value F_{sa} in agile space of parallel mechanism pose setting test is obtained by analyzing different coordinates section in X direction of control point P . Fig. 12 shows the force extremal curves of driving branches. In the simulation, search step of X direction is 0.5mm and r_{step} is 1mm.

It can be seen from Fig. 13, the maximum force values of driving branches during the process of pose setting test of space redocking manipulator end-effector are 2168.62 N and 3251.15 N under the force load F and the moment load M . Because the design load of the single branch ball screw is 6800N, the parallel mechanism satisfies the requirement of the six dimensional composite load bearing capacity of end-effector pose setting test.

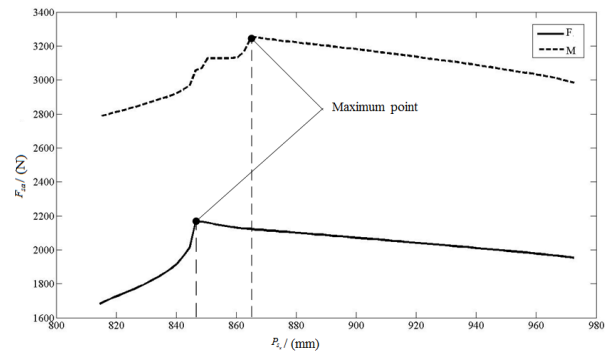


Figure 13. Force extremal curves of driving branches

VI. CONCLUSION

In this article, a pose setting method of space station redocking manipulator end-effector based on parallel mechanism is proposed. The structure and working principle of designed 6-DOF parallel mechanism are presented. The mathematical models of parallel mechanism agile space, kinematic interference characteristics of actuator and adapter and structural statics are also analyzed and established. We compile the Matlab programs of agile workspace search algorithm base on cylindrical coordinates and interference detection algorithm base on space geometry. Simulation results show that movement ranges of designed parallel mechanism meet the demand of required pose, there is no motion interference during pose setting ground test, mechanism has good bearing capacity, and the method is effective. Future work focuses on optimizing the structure parameters and conducting ground experiment of manipulator end-effector.

REFERENCES

- [1] J. P. Zhou, "Chinese space station project overall vision," *Manned Spaceflight*, vol. 19, no. 2, pp. 1-10, 2013.
- [2] Z. G. Xu, X. L. Bai, J. Y. Wang, et al. "Load carrying capacity test of the space station redocking manipulator based on the equivalent inertia simulation method," *RoBot*, vol. 37, no. 2, pp. 231-236, 2015.
- [3] W. F. Xu, X. D. Du, C. J. Wang, et al. "Determination method of overall technology index for space manipulator," *Chinese Space Science and Technology*, vol. 33, no. 1, pp. 53-60, 2013.
- [4] J. Hwang, E. Wu, A. Bell, et al. "Design of a SPDM-like robotic manipulator system for space station on orbit replaceable unit ground testing - an overview of the system architecture," in *Proc. IEEE International Conference on Robotics and Automation*, 1994, pp. 1286-1291.
- [5] J. McGuire, B. Roberts, "Hubble robotic servicing and deorbit mission: Risk reduction, mitigation, and lessons learned," in *Proc. AIAA Space 2007 Conference*, 2007.
- [6] F. J. Cepollina, R. D. Burns, J. M. Holz, et al. Method and associated apparatus for capturing, servicing, and de-orbiting earth satellites using robotics: U.S. Patent 7,513,459. 2009-4-7.
- [7] M. Oda, S. Nishida, N. Inaba, et al. "A feasibility study of robotic servicing for the Hubble Space Telescope," *i-SAIRAS 2005-The 8th International Symposium on Artificial Intelligence, Robotics and Automation in Space*. 2005, 603: 9.
- [8] Lozino-Lozinsky, A. G. Bratukhin, "Aerospace systems: Book of technical papers," Moscow, Russia: Publishing House of Moscow Aviation Institute, 1997.
- [9] B. J. Chen, H. Nie, Y. G. Chen, et al. "The design and key techniques of end-effector for space robot manipulator," *Journal of Astronautics*, vol. 34, no. 12, pp. 1529-1539, 2013.

- [10] L. Shen, X. T. Wang, "Design of high reliability control system for end effector," *Electronic Design Engineering*, vol. 20, no. 15, pp. 78-81, 2012.
- [11] A. El Habachi, S. Duprey, L. Cheze, et al. "A parallel mechanism of the shoulder—application to multi-body optimization," *Multibody System Dynamics*, vol. 33, no. 4, pp. 439-451, 2015.
- [12] J. Arata, H. Kondo, N. Ikedo, et al. "Haptic device using a newly developed redundant parallel mechanism," *IEEE Transactions on Robotics*, vol. 27, no. 2, pp. 201-214, 2011.
- [13] J. M. Prajapati, "Kinematics of parallel mechanism based robot manipulator with passive joints variables," *International IEEE Conference on Control, Automation and Robotics*, 2015.
- [14] G. Gogu, "Structural synthesis of parallel robots," Dordrecht: Springer, 2008.
- [15] H. Q. Le, N. M. Thanh, V. Glazunov, et al. *Screws on the Relative Parallel Mechanisms*, 2014, pp. 221-226.
- [16] D. X. Zeng, J. Wen, Z. Huang, "Over-constraint and a unified mobility method for general spatial mechanisms part 1: essential principle," *Chinese Journal of Mechanical Engineering*, 2015, vol. 28, no. 5, pp. 869-877.



XinLin Bai (Shenyang, China, 1989-), master's degree in mechatronic engineering from University of Chinese Academy of Sciences. Research area: robot mechanism and structure design, ground test of space mechanism, modeling and simulation of robot kinematics and dynamics.

He is currently an assistant researcher at State Key Laboratory of Robotics, Shenyang Institute of Automation, Chinese Academic of Sciences.

Mingyang Liu (Shenyang, China, 1988-), master's degree in flight vehicle design from Harbin Institute of Technology. Research area: space robot motion control, high precision dynamic torque control.

He is currently an assistant researcher at State Key Laboratory of Robotics, Shenyang Institute of Automation, Chinese Academic of Sciences.

Zhigang Xu (Shenyang, China, 1971-), professor, doctoral supervisor, doctor's degree in mechatronic engineering from University of Chinese Academy of Sciences. Research area: special robot mechanism and structure design, ground test of space mechanism, robot cooperation and compliance control.

He is currently an professor at State Key Laboratory of Robotics, Shenyang Institute of Automation, Chinese Academic of Sciences and University of Chinese Academy of Sciences. He published more than 100 papers and 160 patents.

Meng Yin (Shenyang, China, 1991-), doctoral student, University of Chinese Academy of Sciences. Research area: new generation human-machine cooperation manipulator and control system.